

# Metal Oxide-Coated Polymer Nanofibers

Christopher Drew,<sup>†</sup> Xin Liu,<sup>†</sup> David Ziegler,<sup>‡</sup> Xianyan Wang,<sup>†</sup>  
Ferdinando F. Bruno,<sup>‡</sup> James Whitten,<sup>†</sup> Lynne A. Samuelson,<sup>\*‡</sup> and  
Jayant Kumar<sup>\*†</sup>

*Department of Chemistry and Center for Advanced Materials, University of Massachusetts, 1 University Avenue, Lowell, Massachusetts 01854, and Natick Soldier Center, U.S. Army Soldier, Biological, Chemical Command, Natick, Massachusetts*

Received October 16, 2002; Revised Manuscript Received December 6, 2002

## ABSTRACT

We report the fabrication of novel metal oxide-coated polymeric nanofibers using the electrospinning technique. Polyacrylonitrile fibers were electrospun into a nonwoven fiber membrane. The membranes were subsequently immersed in an aqueous solution of metal halide salts and halogen scavengers at room temperature to apply the metal oxide coating. Tin dioxide and titanium dioxide were both successfully coated by this method. Coated fibers were characterized by scanning electron microscopy, transmission electron microscopy, and energy-dispersive X-ray spectroscopy. Glass slides were coated with metal oxides by the same technique and were analyzed by X-ray photoelectron spectroscopy to determine the metal oxide surface composition. Fiber diameters were on the order of 100 nm, and the observed coating thickness ranged from about 20 to 80 nm.

Metal oxides are of great interest because of their chemical and electrical properties. Tin oxide is a known electrical conductor that is optically transparent in the visible spectrum. It is used in photovoltaic cells, liquid crystal displays, and light-emitting diodes. Titanium dioxide is a wide band-gap semiconductor and is known to be a good oxidizing agent for photoexcited molecules or functional groups. As such, titanium dioxide has been widely employed as a photocatalyst,<sup>1–3</sup> as a sensor material,<sup>4,5</sup> and as an electrode in a dye-based photovoltaic cell.<sup>6</sup>

A large interfacial area enhances the desired properties in many of these applications. The interface often is composed of nanometer-scale particles of the metal oxide. In the case of dye-sensitized photovoltaic cells, an additional sintering step is required to ensure maximum electrical connectivity between the metal oxide particles.<sup>7</sup> However, high-temperature sintering limits the possible substrates, such as plastics, that may be employed in fabricating a device.

Electrospinning offers a quick and facile technique to create high-surface-area fiber membranes where the fibers are several orders of magnitude smaller than those produced by conventional spinning techniques.<sup>8</sup> The process uses a high static voltage to create a strong electric field and to impart a small amount of charge into a viscous polymer solution. This combination creates fine jets of the polymer solution that dry into fibers with diameters typically on the order of 100 nm or less. Holman et al. have recently

presented theories and a model for the solution behavior in the electric field.<sup>9</sup> A study of the effects of applied voltage and viscosity on the fiber morphology was presented by Fong et al.<sup>10</sup> It is believed that surface-area-dependent applications such as sensors and catalysts can be greatly improved by taking advantage of the large surface area inherent in electrospun membranes. Wang et al. have recently demonstrated improvements in the sensitivity of fluorescing sensors of an order of magnitude or more by assembling the components in an electrospun membrane.<sup>11</sup>

We have used electrospun fiber membranes as a substrate for a solution deposition of continuous thin coatings of titanium dioxide (TiO<sub>2</sub>) and tin dioxide (SnO<sub>2</sub>). Metal oxide coatings on nanofibrous structures were created by a technique known as liquid-phase deposition, wherein a metal precursor is first hydrolyzed in an aqueous solution and then subsequently forms a metal oxide by the condensation of water. Liquid-phase deposition has been reported for titanium dioxide coatings of flat surfaces.<sup>12</sup> We have successfully extrapolated this technique to create tin dioxide coatings by analogous chemical reactions. This technique readily coated the electrospun fibers without binding them together, thus leaving the inherent high surface area of the electrospun membrane intact.

Polyacrylonitrile (PAN) with a number-average molecular mass of 86 200 D was dissolved in *N,N*-dimethyl formamide (DMF) to form a spin-dope solution of 7.5 wt % of polymer. All chemicals and polymers were obtained from Aldrich Chemical Co. unless otherwise indicated. The charged electrode from a DC power supply (Gamma High Voltage Research, Inc. model HV ES 30P/100) was inserted into a

<sup>†</sup> University of Massachusetts.

<sup>‡</sup> Natick Soldier Center.

pipet containing the spin dope, and the voltage was increased to about 15 kV. The resulting electrospun fibers were collected on an electrically grounded target of either aluminum foil or copper-grid sample holders for use in a transmission electron microscope (TEM).

The electrospun fibers were collected on the target as a membrane of randomly oriented fibers. To expel as much residual solvent as possible, the membranes were heated at 50 °C for 2 h and allowed to cool for at least 6 h prior to their use in the metal oxide coating procedures.

To form the titanium dioxide coating, equal volumes of aqueous 0.12 M hexafluorotitanate(IV) ammonium ( $\text{TiF}_6(\text{NH}_4)_2$ , Strem Chemicals) and 0.2 M boric acid ( $\text{H}_3\text{BO}_3$ ) were combined. The substrates to be coated—either the electrospun nanofiber polymer membranes or the tin oxide-coated glass slides—were then immersed in this mixture for 12 to 36 h. The reaction of hexafluorotitanate(IV) ammonium with water in solution has been reported as an equilibrium between  $\text{TiF}_4$  and  $\text{Ti}(\text{OH})_x\text{F}_y$ , where  $x + y = 4$ .<sup>11</sup> Boric acid serves to consume the hydrofluoric acid in solution, shifting the equilibrium toward the titanium hydroxy product. The subsequent condensation of water results in titanium dioxide formation. Tin dioxide coatings were similarly created by mixing equal volumes of aqueous 0.12 M hexafluorostannate(IV) ammonium ( $\text{SnF}_6(\text{NH}_4)_2$ ) and 0.2 M boric acid ( $\text{H}_3\text{BO}_3$ ) and then immersing the substrates in the solution. Tin dioxide coatings were also formed on nanofiber polymer membranes and glass microscope slides. Tin dioxide coatings were examined after coating times of 12 to 28 h. Electrospun fiber membranes were characterized by scanning electron microscopy (SEM) using an AMRAY model 1400 microscope (accelerating voltage 10 kV) and by transmission electron microscopy (TEM) (JEOL model 2010 FasTEM, accelerating voltage 200 kV). The chemical compositions of the fiber coatings were analyzed by energy dispersive spectroscopy (EDS) (EDAX Corp. SiLi detector) in the TEM.

Uncoated PAN fibers are shown in the top SEM image in Figure 1. As is typical for electrospun fibers, there was a distribution of fiber diameters, and the fibers were randomly oriented as a porous membrane. Titanium dioxide-coated fibers made by a 24-h coating time can be seen in the middle image in Figure 1. The bottom image in Figure 1 shows fibers coated with tin dioxide that were also made by a 24-h coating time. In the case of both tin dioxide- and titanium dioxide-coated samples, the fibers remained discrete, and the membranes, porous and of high surface area.

Although it was difficult to identify the metal oxide coatings in the SEM images, the coatings were readily observed in TEM images. Figure 2A shows an uncoated PAN fiber. The tin dioxide coating on the electrospun fiber, after a 12-h deposition time, is shown in Figure 2B. The coating appears to have covered the fiber completely, with some additional spherical tin dioxide particles having formed on the fiber surface and next to the fiber. These spherical particles are believed to be the result of the nucleation processes from the coating reaction. Although the tin dioxide coating thickness is not clear in the image, if we assume that nucleation sites occurred roughly simultaneously in the

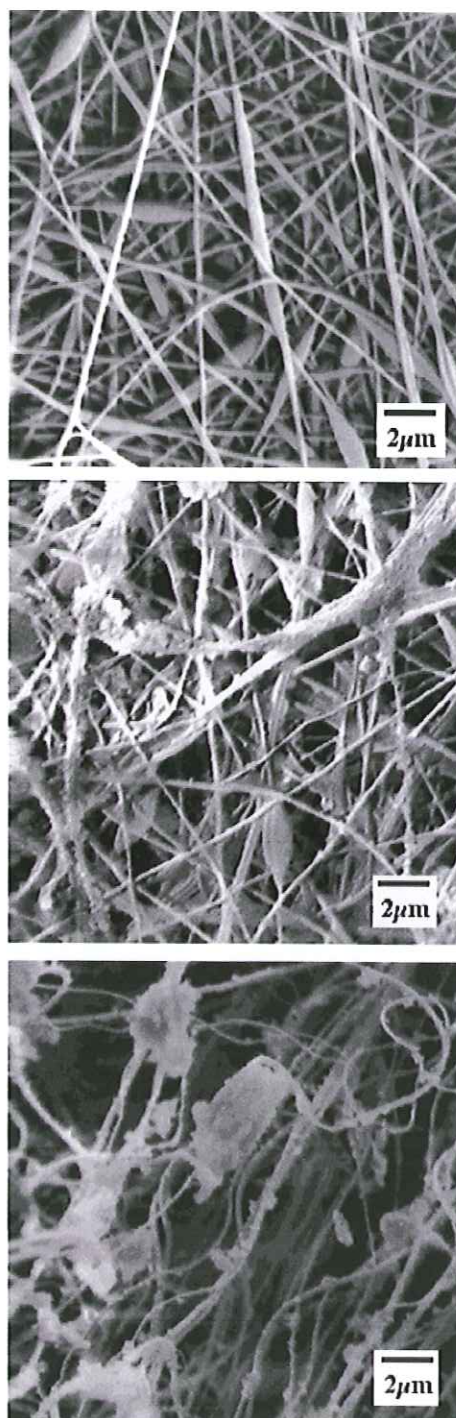
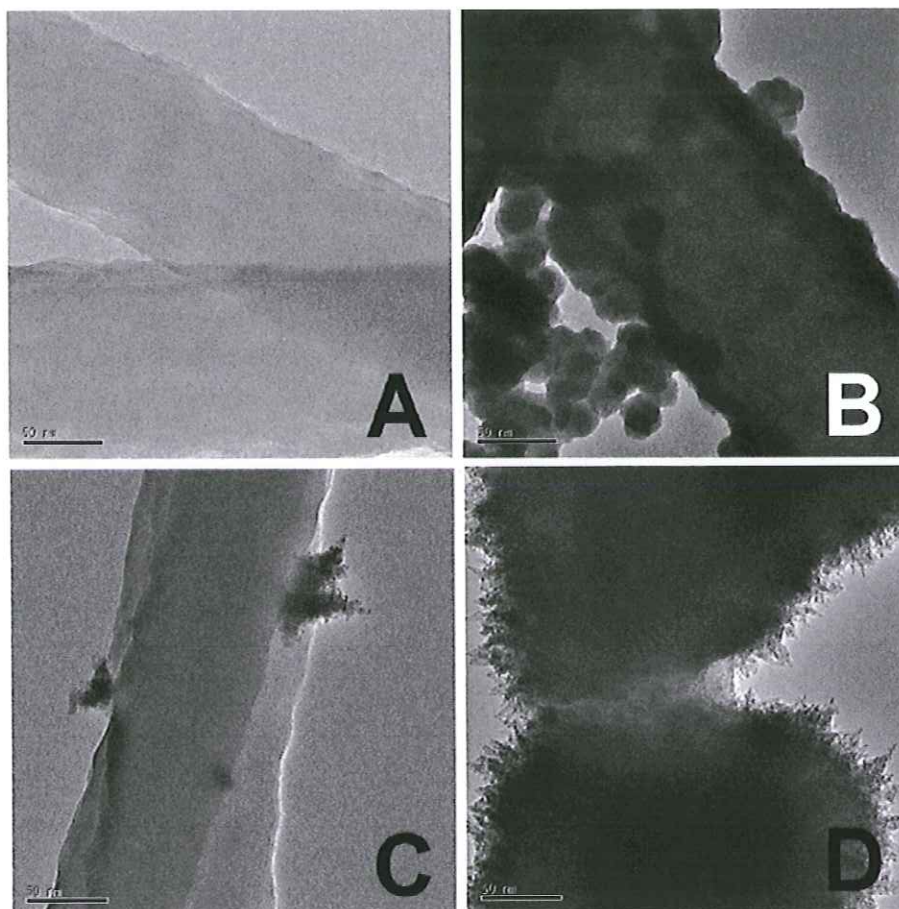


Figure 1. SEM images: Uncoated PAN fibers (top),  $\text{TiO}_2$  coated PAN fibers (middle), and  $\text{SnO}_2$  coated PAN fibers (bottom).

solution and on the fiber surface and that the metal oxide growth was uniform, then the coating thickness on the fiber should be approximately equal to the radius of the particles, which was about 10–15 nm.

A TEM image of a fiber sample coated with titanium dioxide for the same amount of time is shown in Figure 2C. The  $\text{TiO}_2$  coating was observed only as several dendritic-



**Figure 2.** TEM images: (A) Uncoated fibers (B) tin dioxide-coated fibers (12 h), (C) titanium dioxide-coated fibers (12 h), and (D) titanium dioxide-coated fibers (36 h).

shaped particles on the fiber surface. A longer coating time of 36 h for titanium oxide yielded a continuous fiber coating similar to that observed on the tin oxide-coated fibers. Fibers coated for an additional 24 h in the titanium oxide solution are shown in Figure 2D. The  $\text{TiO}_2$  thickness is clearly evident in the gap that is shown and was approximately 80 nm.

We believe that the coating reaction first creates nucleation sites of metal oxide on the fiber. As the coating time increased and the condensation reaction continued, the nucleation sites grew together to form a continuous coating. Since the reactant concentrations, ambient conditions, and coating time were the same for both the tin dioxide- and titanium dioxide-coated fibers, the tin dioxide coating reactions would seem to have been faster. This was also supported by the observation of the formation of a white suspension in the tin oxide reaction vessel. Such a suspension was not observed in the titanium oxide coating solution. The reason for this difference in reaction rates is not known. However, it is postulated that the nucleation rate for tin dioxide was higher because either the reactant or the intermediate product was less soluble than the equivalent titanium reactant. Poor solubility can greatly enhance crystal growth whereas good solubility can slow growth because of

the need for solvent molecules to diffuse away from a molecule for crystallization to occur.<sup>13</sup>

Image maps based on EDS data are shown in Figure 3. Tin dioxide from a 12-h deposition time is observed in the lower image. Blue dots represent tin, and yellow dots represent oxygen. The upper image shows titanium dioxide-coated fibers from a 36-h deposition time where titanium is shown in green and oxygen is in yellow. Carbon, from either the polymer or from contamination, is shown in red in both images. The high concentration of metal and oxygen on the fibers demonstrates the successful application of the metal oxides on the fiber surfaces. The precise composition of the metal oxides was determined by X-ray photoelectron spectroscopy experiments.

X-ray photoelectron spectroscopy (XPS) experiments were performed to verify the deposition of titanium dioxide and tin dioxide in a VG ESCALAB II photoelectron spectrometer using  $\text{Mg K}\alpha$  ( $h\nu = 1253.6$  eV) X-rays. Photoelectrons were detected approximately normal to the sample plane, and their kinetic energies were analyzed by a concentric hemispherical analyzer operating in constant-energy detection mode with a pass energy of 20 eV. The substrates were attached to electrically grounded metal sample stubs via copper tape.

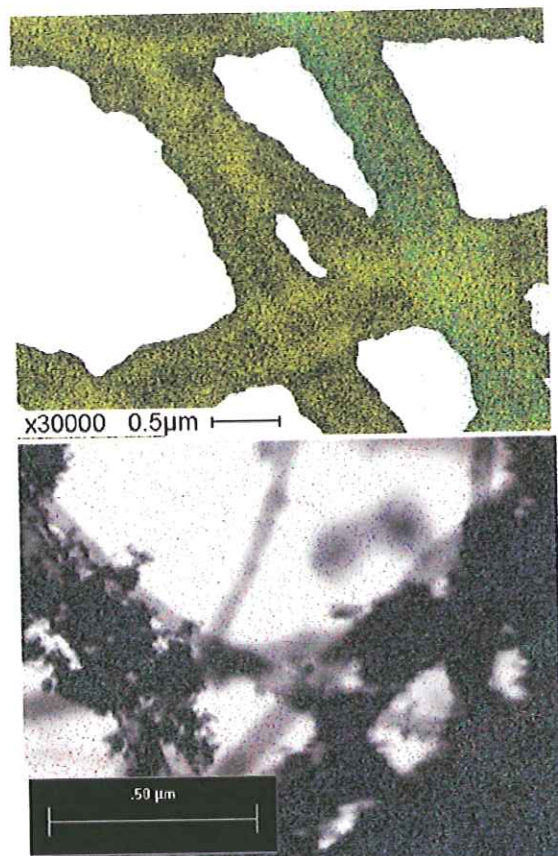


**Figure 3.** X-ray image maps of (top) titanium dioxide- and (bottom) tin dioxide-coated fibers. Sn – blue, Ti – green, O – yellow, and C – red.

Because of the semiconducting/insulating nature of the samples, insufficient grounding and charge compensation caused shifts in the apparent binding energies toward higher values. The adventitious carbon C 1s peak was used as a binding-energy reference, and the spectra for each sample were shifted by a constant value to bring the C 1s peak binding energy to 284.6 eV.

Because of the limited escape depth of photoelectrons and the surface sensitivity, XPS is ideal for measuring the chemistry of surface layers. Figure 4 shows the XPS of the Ti 2p region for a commercially prepared SnO<sub>2</sub> substrate before (spectrum A) and after TiO<sub>2</sub> deposition times of 10 h (spectrum B) and 15 h (spectrum C). The binding energies of the Ti 2p<sub>3/2</sub> and Ti 2p<sub>1/2</sub> peaks at ca. 458 and 464 eV, respectively, are consistent with TiO<sub>2</sub> formation.<sup>14</sup> Spectra from the Sn 3d region of the same samples, with the signal originating from the SnO<sub>2</sub> substrate, are shown in Figure 4. After 10 h of TiO<sub>2</sub> growth, the sample still shows traces of the Sn signal, but after 15 h, no Sn 3d intensity is detectable. The kinetic energy of Sn 3d Mg K $\alpha$ -ejected photoelectrons is ca. 800 eV, which corresponds to a mean free path of about 15 Å.<sup>15</sup> Assuming a detection limit of 1 atom %, the absence of the Sn 3d signal in spectrum C of Figure 4 indicates that the TiO<sub>2</sub> layer was at least 70 Å thick and completely covered the substrate. Elemental analysis of the 15-h TiO<sub>2</sub> sample yielded the following atomic percent-

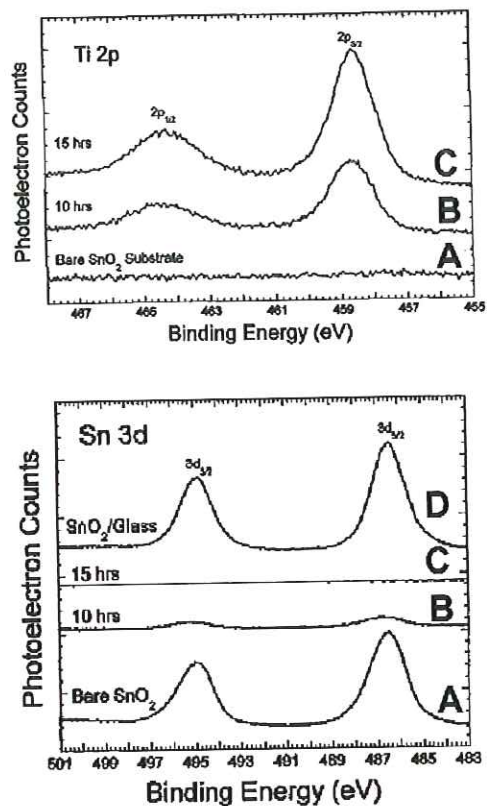


**Figure 4.** XPS spectra of Ti and Sn regions for TiO<sub>2</sub> deposition onto commercial tin oxide-coated glass and SnO<sub>2</sub> deposition onto glass. (A) Commercially prepared tin oxide-coated glass (B) TiO<sub>2</sub> coating by a 10-h deposition time, (C) TiO<sub>2</sub> coating by a 15-h deposition time, and (D) SnO<sub>2</sub> deposition for 28 h.

ages: 43% O, 38% C, 11% Ti, and 7% F. Some of the carbon signal may be due to C-containing contamination, which was present on the bare SnO<sub>2</sub> substrate (as confirmed by XPS), since the kinetic energy of the C 1s photoelectrons is somewhat higher than that from the Sn 3d core level and the escape depth is slightly greater. Most likely, however, the carbon originates from impurities on the surface. Similarly, the fact that the O/Ti atomic ratio is greater than 2.0 is indicative of surface impurities or water adsorption. The fluorine arose from incomplete halogen scavenging during the coating reaction.

Figure 4 (spectrum D) also includes a spectrum of the Sn 3d region for a SnO<sub>2</sub> coating deposited on bare glass by a 28-h coating time. The peaks at binding energies at ca. 486 and 495 eV indicate the formation of SnO<sub>2</sub> on the glass surface. In this case, the elemental composition as measured by XPS was 48% O, 22% C, 20% Sn, and 10% F. That the O/Sn ratio was about 2 and the O/Ti ratio was not quite 4 may be attributable to the difference in solubilities as mentioned above, in addition to a difference in the level of impurities. A more soluble titanium intermediate may have permitted the inclusion of water in the lattice, leading to less condensation than in the tin dioxide sample. Crystal growth from dilute solutions is similar to the stepwise incorporation of molecules in vapor deposition, except that the greater percentage of impurities present can create a higher incidence

of crystal flaws.<sup>13</sup> It is conceivable that a large number of lattice flaws could have led to a larger oxygen presence in the coating. Stoichiometric control is currently being studied.

The liquid-phase deposition of continuous films of both titanium dioxide and tin dioxide have been successfully demonstrated for the first time on the surface of nanometer-scale electrospun polymer fibers. The composition of the metal oxide coatings was confirmed by XPS spectra. The coatings were thin enough to maintain the discreteness of the nanofibers, thereby retaining the large surface area of the electrospun membrane. Such metal oxide-coated nanofibrous membranes are expected to provide unusual and highly reactive surfaces for improved catalysis, sensing, and photoelectric conversion applications.

**Acknowledgment.** We are grateful to Dr. Lian Li for his help in creating the electrospinning setup and the U.S. Army Natick Soldier Center for supporting this research.

### References

- (1) Negishi, N.; Takeuchi, K. *Thin Solid Films* **2001**, *392*, 249–253.
- (2) Fujishima, A.; Honda, K. *Nature (London)* **1972**, *238*, 37–38.

- (3) Watanabe, T.; Nakajima, A.; Wang, R.; Minabe, M.; Koizumi, S.; Fujishima, A.; Hashimoto, K. *Thin Solid Films* **1999**, *351*, 260–263.
- (4) Zhu, Y. a.; Shi, J.; Zhang, Z.; Zhang, C.; Zhang, X. *Anal. Chem.* **2002**, *74*, 120–124.
- (5) Shatalov, I. A.; Zavarin, I. S.; Zaitsev, N. K.; Malkin, J. N. *J. Photochem. Photobiol., A* **1996**, *94*, 63–66.
- (6) O'Regan, B.; Grätzel, M. *Nature (London)* **1991**, *353*, 737–739.
- (7) Grätzel, M. *Curr. Opin. Colloid Interface Sci.* **1999**, *4*, 314–321.
- (8) *Kirk-Othmer Encyclopedia of Chemical Technology*, 4th ed.; Kroschwitz, J. I., Howe-Grant, M., Eds.; Wiley: New York, 1991; Vol. 10.
- (9) Hohman, M.; Shin, M.; Rutledge, G.; Brenner, M. *Phys. Fluids* **2001**, *13*, 2201–2220.
- (10) Fong, H.; Chun, I.; Reneker, D. H. *Polymer* **1999**, *40*, 4585–4592.
- (11) Wang, X.; Drew, C.; Lee, S.-H.; Senecal, K. J.; Kumar, J.; Samuelson, L. A. *Nano Lett.* **2002**, *2*, 1273–1275.
- (12) Shimizu, K.; Imai, H.; Hirashima, H.; Tsukuma, K. *Thin Solid Films* **1999**, *351*, 220–224.
- (13) Doremus, R. H. *Rates of Phase Transformations*; Academic Press: New York, 1985.
- (14) Wagner, C. D.; Riggs, W. M.; Davis, L. E.; Moulder, J. F.; Muilenberg, G. E. *Handbook of X-ray Photoelectron Spectroscopy*; Perkin-Elmer Corporation: Eden Prairie, MN, 1979.
- (15) Feldman, L. C.; Mayer, J. W. *Fundamentals of Surface and Thin Film Analysis*; North-Holland: New York, 1986.

NL025850M